Arabian Journal of Chemistry (2023) **16**, 105159

King Saud University

Arabian Journal of Chemistry

www.ksu.edu.sa
www.sciencedirect.com

ORIGINAL ARTICLE

Leaching of cuprite with ozone as an oxidant in sulfuric acid solution and its oxidation leaching mechanism

Jing Yang [b], Luzheng Chen [b], Dandan Wu [a,*], Jing Cao [a], Jinfu Guo [a]

[a] *State Key Laboratory of Complex Non-ferrous Metal Resources Clean Utilization, Kunming University of Science and Technology, Kunming 650093, China*
[b] *Faulty of Land Resource Engineering, Kunming University of Science and Technology, Kunming 650093, China*

Received 8 May 2023; accepted 8 July 2023
Available online 13 July 2023

KEYWORDS

Cuprite;
Oxidation leaching;
Ozone;
Sulfuric acid

Abstract Leaching has been an effective method for extracting copper from cuprite, but disproportionation reaction occurs in its acid leaching process and forms copper ions and copper elements, which results in the highest leaching rate available reaching only 50%. In this investigation, ozone was used to oxidize the cuprite to improve its leaching rate in a sulfuric acid solution, and its oxidation leaching mechanism was proposed and verified via various characterizations. The leaching test results indicated that when the temperature, acid concentrate and stirring speed were kept at constant of 50 °C, 0.014 mol/L, 800 rpm, respectively, the leaching rate of cuprite significantly increased by 43.24% with the increase of the ozone ventilation volume from 0 L/min to 3.0 L/min. Moreover, the leaching process of cuprite controlled by mixed steps and the reaction activation energy was 31.51 kJ/mol. The atomic force microscope observation revealed a noticeable alteration in the surface morphology of cuprite after oxidation leaching. The peak height experienced a significantly decrease, indicating that the oxidation leaching reaction was intensified. The analyses from the X-ray diffraction, X-ray photoelectron spectroscopy, scanning electron microscopy-energy dispersive spectroscopy and time-of-flight secondary ion mass spectrometry indicated that copper elements formed during the direct leaching of cuprite due to the disproportionation reaction, while most Cu_2O were dissolved during the oxidation leaching process. When ozone was added, the Cu^{+} on the cuprite surface was oxidized to Cu^{2+}, and each newly generated CuO film was timely dissolved in the sulfuric acid. It is thus concluded that ozone effectively oxidized cuprite, strengthened its leaching process, and significantly increased its leaching rate. The

* Corresponding author.
E-mail address: wdd1006530@sina.com (D. Wu).
Peer review under responsibility of King Saud University.

Production and hosting by Elsevier

https://doi.org/10.1016/j.arabjc.2023.105159

findings of this study might provide a green approach for the effective oxidation leaching of cuprite.

1. Introduction

Cuprite (Cu_2O) is one of the main copper oxides with copper content reaching as high as 88.82%, and it has a high industrial value. The main methods for utilizing cuprite include flotation and leaching (Bai et al., 2018; Han et al., 2021a; Han et al., 2021b; Sheng et al., 2018). When the sulfidation-xanthate flotation method was used to concentrate cuprite, it is difficult for sulfur ions in sodium sulfide to react with monovalent copper in cuprite, from the thermodynamic point of view (Han et al., 2021c). Therefore, a sulfide film was not easily formed on the cuprite surface, and consequently it is difficult for the xanthate collector to be adsorbed on the cuprite surface and to produce a satisfactory flotation performance (Sheng et al., 2021). It was ever reported that the sulfidation-xanthate flotation method achieved an impromved flotation performance with recovery reaching 75% by pre-oxidizing the cuprite (Han et al., 2021c; Han et al., 2021d; Han et al., 2021e), but this performance was still not so satisfactory.

Leaching is another method for the recovery of cuprite. Aracena et al. has studied the leaching of cuprite in an ammoniacal medium (Aracena et al., 2018), and it was found that its leaching rate reached 82% under conditions such as pH = 10.5, NH_4OH concentration = 0.10 mol/L, leaching temperature = 45 °C, leaching time = 4 h, stirring speed = 850 rpm, and liquid–solid ratio = 400:1. They believed that this improvement in the leaching rate was due to the formation of $Cu(NH_3)_4^{2-}$ in the solution. Generally, the ammoniacal medium is effective for leaching the cuprite, but its disadvantages, such as the long leaching time and the relatively low leaching rate, restrict its effective and economic applications. For the acid leaching process, sulfuric acid or hydrochloric acid is mainly adopted to extract copper from the cuprite. The acid leaching equation is as follows (Aracena et al., 2018):

$$Cu_2O + 2H^+ = Cu^{2+} + Cu^0 + H_2O \quad (1)$$

It is clear from Eq. (1), the disproportionation reaction between cuprite and acid occurs and generates copper ions and copper elements, leading to the highest leaching rate available only reaching 50%. In this electrochemical process, the copper (I) in the cuprite needs to be oxidized to obtain electrons so as to improve the leaching rate.

As an important chemical process in the chemical industry (Ge et al., 2022; Su et al., 2022; Tan et al., 2022; Wei et al., 2021; Wu et al., 2022), the oxidation reaction contributed to around 60% of the chemical products production, and the reaction medium has been primarily the volatile organic compounds (Abazari et al., 2021; Bottone et al., 2022; Chen et al., 2022; Cui et al., 2021; Manoli et al., 2022; Sun et al., 2022; Tan et al., 2020). It is noted that the oxidizing agents used in the oxidation process are usually high-state inorganic metal salts and organic compounds with oxidation capacity. However, such chemical processes require high production costs and produce a large amount of hazardous wastes, thereby posing a great threat to the ecological environment. In recent years, with the increasing awareness to environmental protection and green chemistry production, ozone as a clean oxidant and an environment-friendly green chemical reaction medium has attracted more and more attentions (Alrousan and Dunlop, 2020; Baek et al., 2019; Funke et al., 2021).

Ozone (O_3), an allotrope of oxygen, is a molecule composed of three oxygen atoms. The standard oxidation potential value of ozone in an aqueous solution reaches 2.07 V, which is only lower than that (3.06 V) of fluorine, and is considerably higher than those of hydrogen peroxide (1.78 V), potassium permanganate (1.70 V), chlorine (1.36 V) and oxygen (1.23 V) (Martinez et al., 2022). It exerts a strong oxidation effect in the chemical reaction process. Compared with other traditional oxidants, ozone oxidation avoids the introduction of new impurities in the oxidation system, such as potassium permanganate, manganese dioxide, fluorine and chlorine, as well as the excessive expansion of the solution system during the oxidation process of hydrogen peroxide. Obviously, ozone possesses advantages, such as high oxidation efficiency and selectivity, simple operation, and wide application ranges; and, the oxygen produced from the ozone oxidation process causes no pollution to the surroundings. Due to these advantages over other traditional oxidants, ozone oxidation technology has been widely used in the field of hydrometallurgy (Gui et al., 2022; Gomes et al., 2022; Lv et al., 2021; Xin et al., 2021; Zhang et al., 2022).

In this study, ozone was for the first time attempted as an oxidant for the oxidation leaching of cuprite in a sulfuric acid solution, and its leaching mechanism was fully elucidated using atomic force microscope (AFM), X-ray diffraction (XRD), X-ray photoelectron spectroscopy (XPS), scanning electron microscopy-energy dispersive spectroscopy (SEM-EDS), and time-of-flight secondary ion mass spectrometry (ToF-SIMS). This study aimed to provide a theoretical basis for enhancing the acid leaching process of cuprite.

2. Materials and methods

2.1. Materials

The cuprite sample used in this investigation was obtained from Thaysombon Province, Laos. After hand sorting, crushing, grinding, and screening, the sample with a particle size of 38 ~ 45 μm was obtained. The chemical analysis of cuprite is presented in Table 1. As shown in the Table, the sample contains 88.53% Cu and small amounts of alumina and quartz.

2.2. Leaching experiments

The leaching process was carried out in a 500 mL three-flask batch reactor, with a thermostat to maintain the temperature of the leaching solution during the reaction process. The reactor was equipped with a digitally controlled mechanical agitator, a condenser to prevent evaporation loss, and a rubber cap with vents. Ozone was generated from an ozone generator, and its ventilation volume was controlled at a given level using a flowmeter. A cuprite sample of 5.0 g was added to the deionized water, and then ozone was injected into the suspension. After 3 min of oxidation, sulfuric acid solution was added to this suspension and ozone was continuously injected during this process. According to the preset leaching time, 5 mL of the leaching solution was removed from the upper layer of the leaching solution, and the concentration of copper ions in the solution was measured through inductively coupled plasma-atomic emission spectroscopy so as to calculate the leaching rate x of copper. In the leaching experiments, the

Table 1 Chemical compositions of pure cuprite.

Compositions	Cu	Al_2O_3	SiO_2	Fe	MgO
Contents (%)	88.53	0.80	0.57	0.15	0.048

Table 2 Leaching parameters and ranges used in leaching experiments.

Parameter	Value
Ozone ventilation volume (L/min)	1.0, 1.5, 2.0, 2.5, 3.0*
Leaching temperature (°C)	20, 30, 40, 50*, 60
H_2SO_4 concentration (mol/L)	0.008, 0.010, 0.012, 0.014*, 0.016
Stirring speed (rpm)	200, 400, 600, 800*, 1000

*These parameters were kept constant.

effects of ozone ventilation volume, temperature, H_2SO_4 concentration and stirring speed were focused to be studied, and the values are shown in Table 2.

2.3. Description of characterization methods

2.3.1. AFM detection

The Dimension Icon of Bruker AXS (USA) was used for the AFM test. It is equipped with a probe, which compose of a triangular cantilever (SCANA SYST-Air; thickness = 650 nm; length = 115 μm; width = 25 μm, frequency = 70 kHz; spring const = 0.4 N/m), a tetrahedral needle tip (Silicon Nitride, tip radius = 2 nm, tip hight = 2.5–8.0 μm) and a base. A pixel of 256 lines, a scan rate of 1 Hz, and a scan area of 5×5 μm^2 were chosen to ensure that the images obtained had sufficient resolution and reliable mechanical property mapping.

2.3.2. XRD detection

The X-ray source used for the XRD test was copper target Kα ray, with a wavelength of 0.154056 nm, and the tube current and voltage were set at 40 mA and 40 kV, respectively. With a θ–2θ step-scan method, the analysis was performed in the range of 10°–90°, using a graphite monochromator filter at a scanning speed of 3°/min.

2.3.3. XPS measurement

X-ray photoelectron spectrometry (PHI 5000, ULVAC-PHI, Japan) was used for the surface analysis of the cuprite sample under different conditions. A polished $1 \times 1 \times 0.1$ cm^3 cuprite slice was used in this measurement. Using Mg-Kα x-ray (1253.6 eV) excitation, the x-ray source power was 200 W, the background vacuum was greater than 10^{-7} Pa, and the energy scale was corrected to the binding energy of contaminant carbon C 1 s at 248.80 eV.

2.3.4. SEM-EDS detection

The surface morphology and energy spectrum of cuprite under different conditions were tested using an SEM-EDS instrument (XL30ESEM-TM). The conditions for this characterization analysis were an acceleration voltage of 15 keV, beam current of 100 pA, working distance of 15 mm, and a vacuum.

2.3.5. ToF-SIMS detection

In this detection, the samples were all detected with ToF-SIMS (ION-TOF, Munster, Germany). The analysis gun used Bi^+ as the primary ion source, operating at a primary energy of 30 keV. The analysis area of the sample was set to 500×500 μm^2, and the measurement time was set to 66 s.

3. Results and discussion

3.1. Leaching investigation

3.1.1. Oxidative leaching reaction and effect of O_3 concentration

Ozone has a strong oxidation capacity and it oxidizes reactants at room temperature. For cuprite, ozone oxidized its monovalent copper to divalent copper, and the oxidation reaction was as follows:

$$Cu_2O + O_3 \rightarrow 2CuO + O_2 \quad (2)$$

After cuprite was oxidized by ozone, cuprous oxide was converted into copper oxide. Then, sulfuric acid in the solution reacted with copper oxide to produce copper sulfate and water, as follows:

$$CuO + H_2SO_4 \rightarrow CuSO_4 + H_2O \quad (3)$$

Thus, the overall oxidation leaching reaction was described as:

$$Cu_2O + O_3 + 2H_2SO_4 \rightarrow 2CuSO_4 + 2H_2O + O_2 \quad (4)$$

For this investigation, six different ozone ventilation volumes (0, 1.0, 1.5, 2.0, 2.5, and 3.0 L/min) were respectively adopted to show the effect of ozone concentration on the cuprite leaching rate. For this purpose, the temperature, sulfuric acid concentration, and stirring speed were kept constant at 50 °C, 0.014 mol/L and 800 rpm, respectively. As shown in Fig. 1, the leaching rate of cuprite was obviously affected by the ozone ventilation volumes, and significantly increased with an increase in the ozone ventilation volume. When the cuprite was directly leached in sulfuric acid, the leaching rate only reached 49.50% after a leaching time of 40 min. However, when the ozone ventilation volume was increased by 3.0 L/min, the leaching rate was significantly increased to 92.74%. Thus, the cuprite leaching rate after oxidation was increased by 43.24% compared with the direct leaching. In this leaching phenomenon using ozone, it was presumed that the concentration of oxidant in the leaching reaction system was increased with the increase in the ozone ventilation volume. This in turn facilitated the conversion of more Cu^+ into Cu^{2+}. Finally, the disproportionation reaction for the cuprite was inhibited, and the cuprite leaching rate was significantly improved. Thus, it was clear that the ozone had a strengthening effect on the leaching reaction for cuprite in the sulfuric acid solution, and the improvement in the ozone concentration contributed to the increased leaching rate of cuprite.

3.1.2. Effect of temperature on the leaching of copper

When maintaining a constant ozone ventilation volume of 3.0 L/min, acid concentration of 0.014 mol/L, and stirring speed of 800 rpm, the experiments were carried out at five different temperatures ranging from 20 °C to 60 °C. As depicted in Fig. 2, the leaching rate increased gradually with the increase in reaction temperature, and in the first 10 min of leaching, the leaching rate increased sharply. After 40 min of leaching, 76.84% of copper was leached at 20 °C and 94.98% at 60 °C. The results of the temperature tests demonstrated that the reaction temperature was one of the important factors affecting the leaching of copper from cuprite.

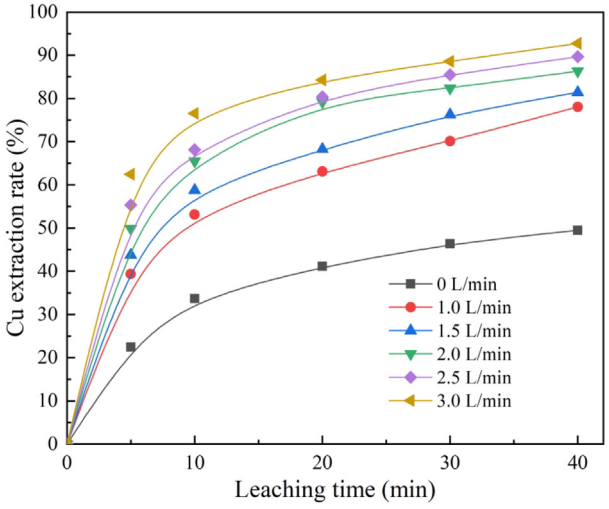

Fig. 1 Effect of ozone ventilation volume on cuprite leaching rate.

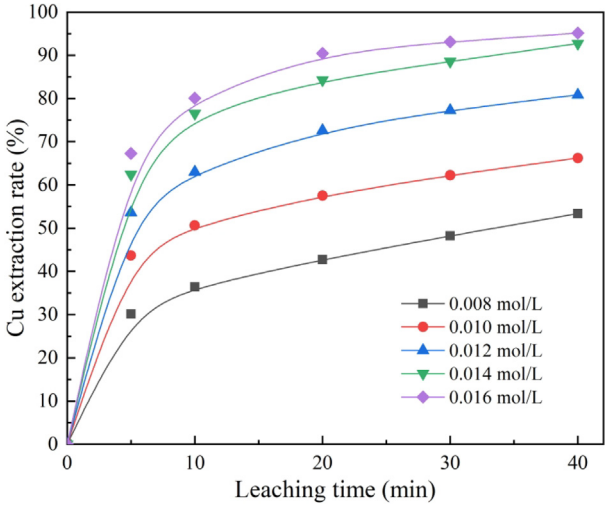

Fig. 3 Effect of H_2SO_4 concentration on cuprite leaching rate.

3.1.3. Effect of H_2SO_4 concentration on the leaching of copper

When the ozone ventilation volume, temperature, and stirring speed were kept at constant of 3.0 L/min, 50 °C, 800 rpm, respectively, the effect of H_2SO_4 concentration on the leaching rate was examined at concentrations of 0.008, 0.010, 0.012, 0.014 and 0.016 mol/L. The results in Fig. 3 illustrated that the leaching rate of copper increased sharply with the increase of H_2SO_4 concentration. After 40 min of the leaching, the leaching rate of copper was 53.36% at H_2SO_4 concentration of 0.008 mol/L. When H_2SO_4 concentration increased to 0.016 mol/L, the leaching rate reached 95.16%. Moreover, when H_2SO_4 concentration exceeded 0.014 mol/L, the leaching rate of copper increased very little. Consequently, H_2SO_4 concentration dramatically affected the cuprite leaching rate.

3.1.4. Effect of stirring speed on the leaching of copper

The effect of stirring speed in the range of 200 to 1000 rpm on copper extraction rate was investigated, and the results are shown in Fig. 4. The experimental conditions consisted of an ozone ventilation volume of 3.0 L/min, an acid concentration of 0.014 mol/L, and a temperature of 50 °C. The results demonstrated that the copper extraction rate gradually increased with the increase in stirring speed. For a stirring speed of 200 rpm, an extraction rate of 79.15% was achieved at 40 min; when the stirring speed increased to 1000 rpm, an extraction rate of 94.35% was achieved at 40 min. The increase in stirring speed accelerated the diffusion of reactants and products in the leaching process, resulting in an increasing leaching rate.

3.1.5. Kinetic analysis

The kinetics of the leaching process of cuprite was explored to find out the factors affecting the leaching rate and understand the control steps of the leaching process. The leaching process can be described as a liquid–solid reaction, and the reaction between solid and fluid can be represented as follows:

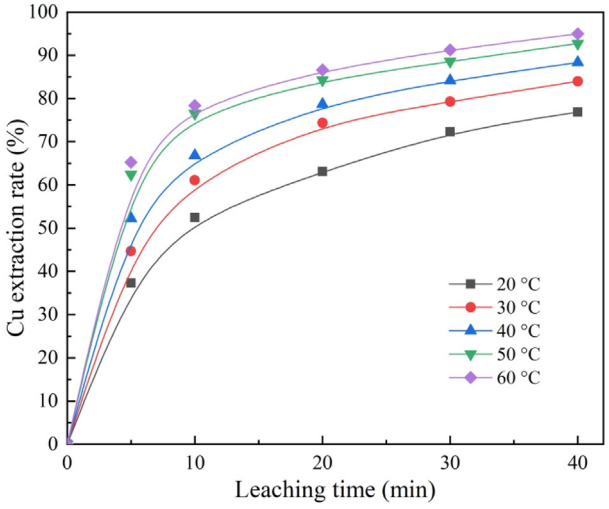

Fig. 2 Effect of temperature on cuprite leaching rate.

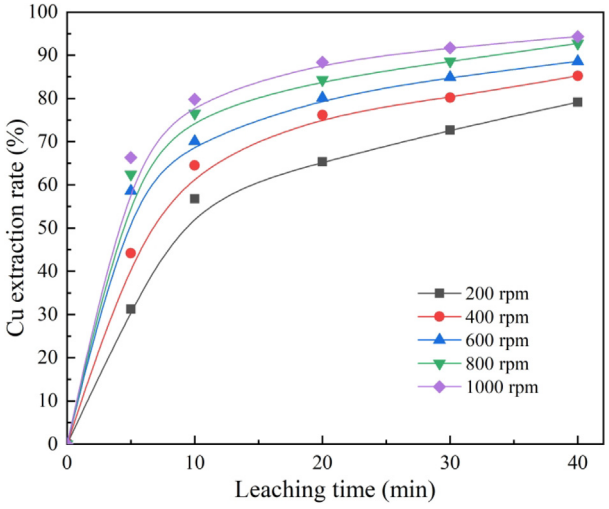

Fig. 4 Effect of stirring speed on cuprite leaching rate.

$$A(s) + B(aq) \rightarrow Products \quad (5)$$

where A and B represent the solid and the liquid reactant undergoing leaching, respectively.

The leaching process of cuprite is in line with the shrinking core model in the leaching kinetics theory (He et al., 2022), which is divided into four control models, namely, the external diffusion link control model (Eq. (6)), the internal diffusion link control model (Eq. (7)), the chemical reaction link control model (Eq. (8)) and the mixed kinetic control model (Eq. (9)). The kinetics equations of the aforementioned four types of models can be written as follows (Ajiboye et al., 2019; Chen et al., 2022; Zhang et al., 2021):

$$x = k_l t \quad (6)$$

$$1 - 3(1-x)^{2/3} + 2(1-x) = k_d t \quad (7)$$

$$1 - (1-x)^{1/3} = k_r t \quad (8)$$

$$1/3\ln(1-x) - 1 + (1-x)^{-1/3} = kt \quad (9)$$

where x is the leaching rate, t is the reaction time, and k_l, k_d, k_r and k are the related apparent rate constants of the leaching reaction.

To find the rate-controlling step of the leaching of cuprite in sulfuric acid solutions, the kinetic parameters were analyzed based on the shrinking core model using the rate expressions given in Eqs. (6)–(9). Based on the analysis results, the model in Eq. (9) could be more suitable to demonstrate the kinetics for this leaching system. The apparent rate constant, linear correlation coefficient, and fitting curve for the mixed kinetic control model are presented in Fig. 5.

As shown in Fig. 5, the linear correlation coefficient R^2 of the mixed kinetic control model was more than 0.99, except for one correlation coefficients slightly lower than 0.99 (0.9795), indicating an excellent linear relationship. Therefore, Eq. (9) was considered as a kinetic model for the leaching process of cuprite.

The kinetics of the leaching process controlled by mixed steps could be expressed as follows:

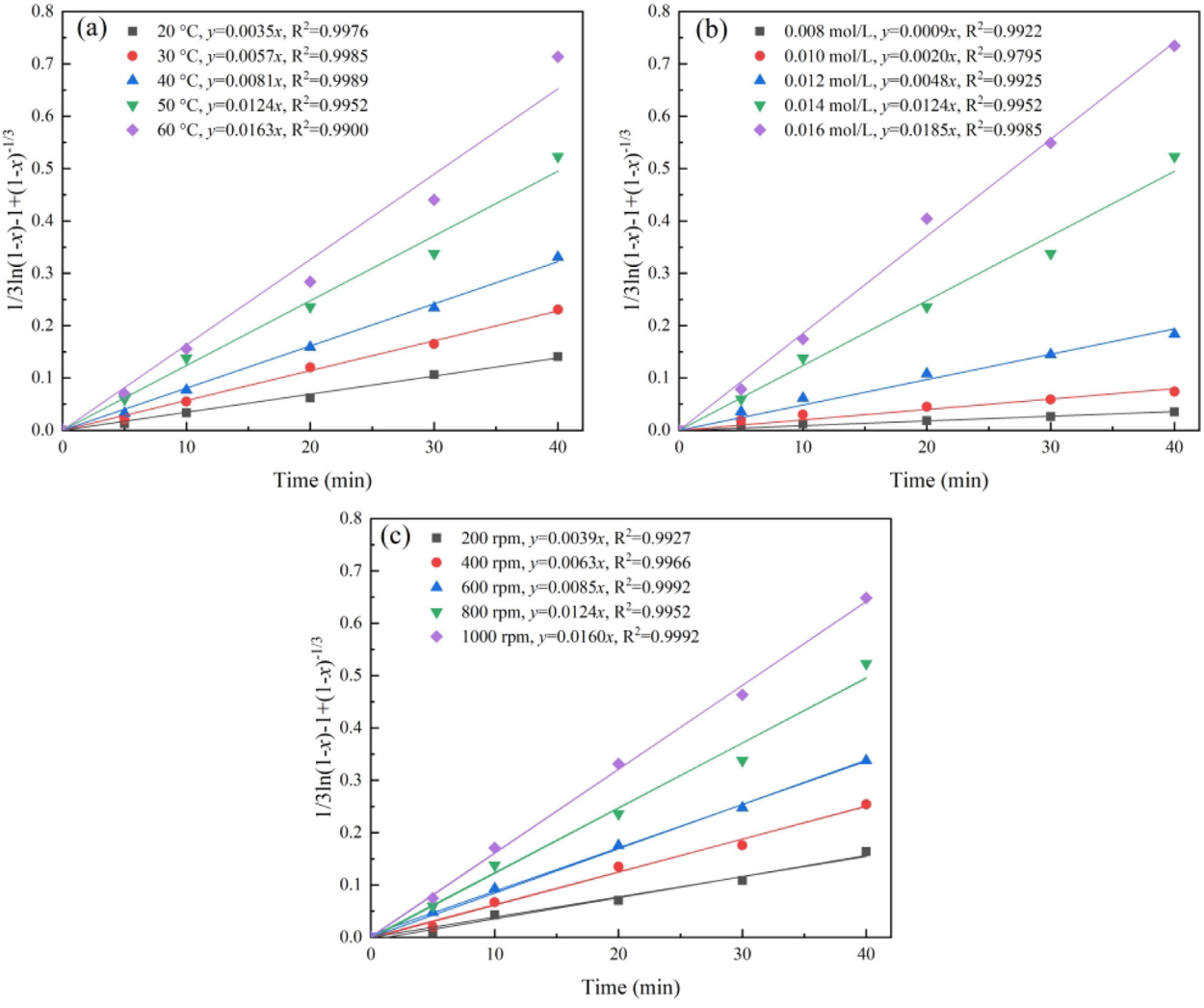

Fig. 5 Fitting curve of $1/3\ln(1-x) - 1 + (1-x)^{-1/3}$ to the three influencing factors: (a) temperature, (b) H_2SO_4 concentration, and (c) stirring speed.

$$1/3\ln(1-x)-1+(1-x)^{-1/3} = \left[k_0\cdot(C)^{\alpha}\cdot(SS)^{\beta}\cdot\exp(-E/RT)\right]\cdot t \quad (10)$$

where, C, SS, E, R and T are the concentration, stirring speed, activation energy, molar gas constant and temperature, respectively. The constants α and β are the dependence of the reaction rate on the relevant parameters, and k_0 is the frequency factor.

The Arrhenius graph of the cuprite leaching process is shown in Fig. 6. The activation energy of cuprite leaching was calculated from Fig. 6 as 31.51 kJ/mol in the temperature range of 20–60 °C and the correlation coefficient of the fitted curve was 0.9962, which also indicated that the leaching of cuprite in the sulfuric acid solution followed the mixed kinetic control model. Fig. 7(a-b) shows the relationship between ln$k$ and ln$C$, and lnSS, respectively. the constants α and β were determined from the slopes of the straight lines, which were 4.5486 and 0.8737, respectively.

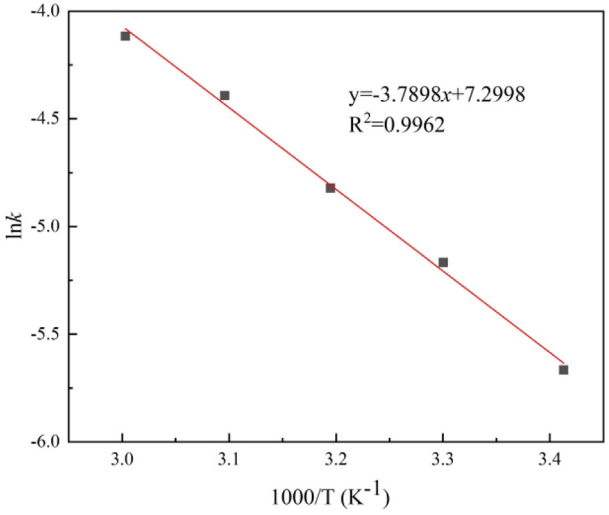

Fig. 6 Arrhenius plot of the dissolution of cuprite.

Therefore, the following kinetic expression could be represented to describe the kinetics equation of cuprite leaching:

$$1/3\ln(1-x)-1+(1-x)^{-1/3} = \left[k_0\cdot(C)^{4.5486}\cdot(SS)^{0.8737}\cdot\exp(-31.51/RT)\right]\cdot t \quad (11)$$

3.2. AFM imaging for raw cuprite, oxidative product and leaching residue

While the distance between atoms was reduced to a certain level, their interatomic force increases rapidly, which lays the basic principle for AFM imaging. Based on the principle, surface imaging is implemented via the force between the microprobe and the sample surface so that the information on the sample surface topography is achievable (Li et al., 2019; Xie et al., 2021; Xing et al., 2018; Zhu et al., 2019). Fig. 8 lists the AFM images for the surface morphology and the changes in the cross-section height for cuprite, cuprite after direct leaching, cuprite after ozonation, and cuprite after oxidation leaching. These images have vividly revealed the erosive effect of leaching agents and oxidants on the cuprite surface. Specifically, Fig. 8(a-c) respectively shows the two-dimensional (2D) geometric topography, cross-section height, and the three-dimensional (3D) height topography of cuprite; and Fig. 8(d-f) respectively shows the 2D geometric topography, cross-section height, and the 3D height topography of directly leached cuprite. It can be seen that when the cuprite reacted with the leaching agent, its surface was eroded and a large number of peaks appeared. After the cuprite was dissolved in sulfuric acid, the height of peaks on the surface reduced from 4.6 nm to 2.1 nm, and the surface morphology has changed. Fig. 8(-g-i) shows the 2D geometric topography, cross-section height, and the 3D height topography of cuprite after ozonation; and, it can be seen that when the cuprite was oxidized by ozone, a layer of copper oxide film was formed on the cuprite surface, leading to that the height of peaks increased from 4.6 nm of cuprite to 12.2 nm of cuprite after ozonation. Fig. 8(j-l) respectively shows the 2D geometric topography, cross-section height, and the 3D height topography of the oxidation leached

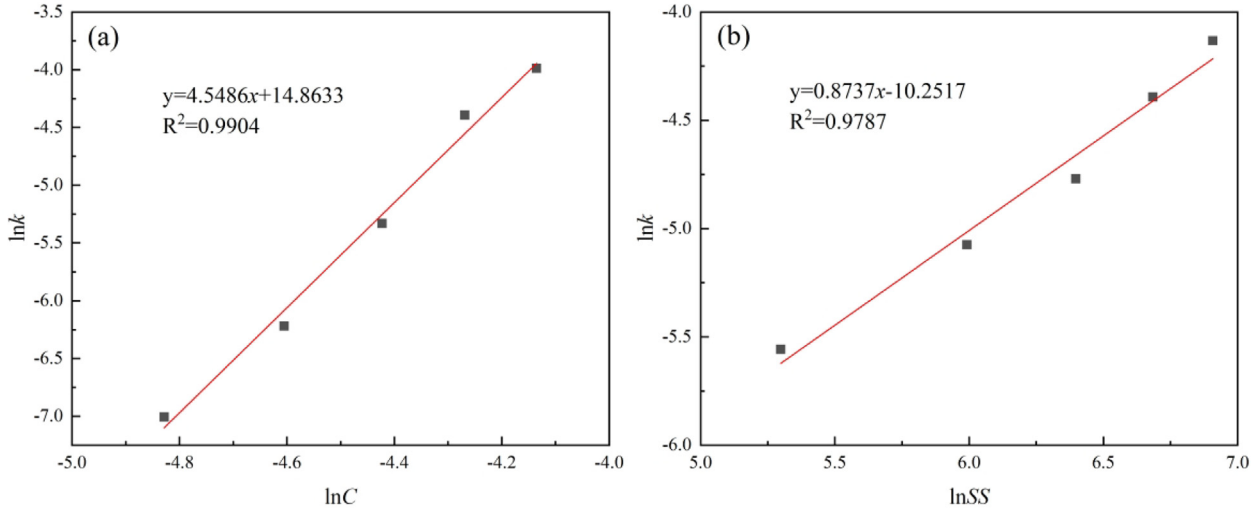

Fig. 7 Plot of ln$k$ versus different influencing factors: (a) reagent concentration and (b) stirring speed.

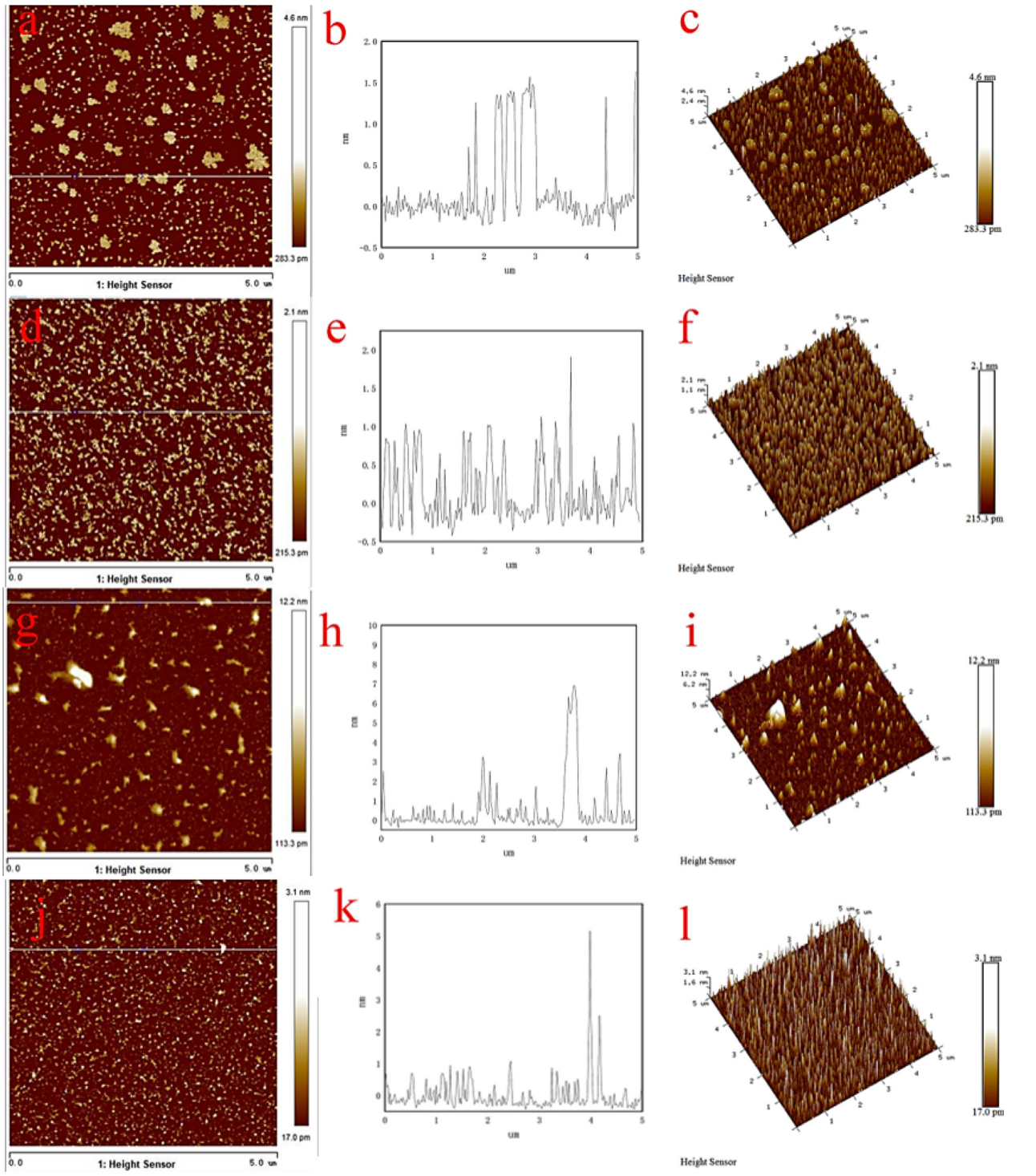

Fig. 8 AFM images of topography on the surfaces of cuprite (a-c), cuprite after reaction with sulfuric acid (d-f), cuprite after reaction with ozone (g-i), cuprite after reaction with ozone and sulfuric acid (j-l).

cuprite; and, it is clear that when the ozone and sulfuric acid were respectively used as oxidant and leaching agent, the cuprite surface was oxidized by ozone to form a copper oxide film, and the copper oxide film was dissolved by sulfuric acid, reducing the height of peaks from 12.2 nm to 3.1 nm.

Comparing the AFM morphologies of cuprite under the aforementioned conditions, it was found that when the cuprite was oxidized by ozone, it had the greatest influence on the height of the cuprite surface peak, and the oxidation leaching had the least influence. Therefore, it was easy to understand that the copper oxide film was formed on the cuprite surface after ozonation, and the peak height on the cuprite surface was greatly increased. The cuprite or the CuO film on the cuprite surface was dissolved in the acid leaching process, so

that the peak height on the cuprite surface after direct leaching or oxidation leaching was lower than that after oxidation. It was seen that the addition of ozone has effectively increased the oxidation reaction efficiency for cuprite, so that the leaching reaction easily occurred, which improved the leaching rate of cuprite.

3.3. XRD analysis for phases of raw cuprite, oxidative product and leaching residue

Fig. 9 shows the XRD test results of cuprite, cuprite after direct leaching, cuprite after ozonation, and cuprite after oxidation leaching. As shown in Fig. 9, the raw cuprite mainly contained cuprite and a small amount of elemental copper. Its diffraction peaks of Cu_2O were sharp and intense, indicating a highly crystalline nature; meanwhile, its extremely low diffraction peak intensity of Cu, indicating the low Cu content in the cuprite. No impurity peaks were observed, further confirming its high purity.

For the cuprite after direct leaching (Cuprite + H_2SO_4 in Fig. 9), the diffraction peak intensity of Cu_2O was decreased slightly due to the dissolution of sulfuric acid, while that of Cu was significantly increased. This phenomenon has further proved that the direct leaching of cuprite is a disproportionation reaction process, in which elemental copper was formed. For the cuprite after ozonation (Cuprite + O_3 in Fig. 9), the diffraction peaks for both Cu_2O and Cu were similar to that for raw cuprite, indicating that a copper oxide film was generated on the cuprite surface during its ozonation process. This copper oxide film hindered the further oxidation of cuprite by ozone, so that the CuO phase was not detected, as clearly shown in Fig. 9. For the cuprite after oxidation leaching (Cuprite + O_3 + H_2SO_4 in Fig. 9), the diffraction peak intensity of Cu was increased significantly while that of Cu_2O was decreased significantly. In this investigation, Cu was observed in the final leaching residue because a small amount of Cu was present in raw cuprite as mentioned earlier, and the disproportionation reaction inevitably occurred in the oxidation leaching process for cuprite. In addition, the leaching residue produced from the oxidation leaching process contained a small amount of Cu_2O, due to the fact that a small amount of cuprite was not fully oxidized, which made its dissolution in sulfuric acid difficult.

3.4. XPS analysis for Cu and O valence states of raw cuprite, oxidative product and leaching residue

In this investigation, XPS was used to measure the Cu and O valence states and reaction products on the cuprite surface during the sulfuric acid leaching process in the absence and presence of O_3. The XPS curve-fitting spectra for O1s of cuprite under different conditions are shown in Fig. 10. Fig. 10a shows the O1s curve-fitting spectra on the untreated cuprite surface. Two peaks could be fitted from the binding energy of O1s, with the peaks at 532.31 eV and 530.92 eV corresponding to water and metal oxides, respectively (Marchon et al., 1988; Poulston et al., 1996; Scandurra et al., 2021). It is noted that the high peak height of water in Fig. 10a might be resulted from the sensitivity of cuprite to hydration, which led to the existence of combined water in the mineral during the sample preparation while stirring it with deionized water. Even after drying, the water remained in the cuprite, and thus the peak area grew larger. Fig. 10b shows the O1s curve-fitting spectra of the cuprite surface after sulfuric acid leaching. It was clear that the spectral peak of water reached 532.14 eV, and this is 530.83 eV for metal oxide (Poulston et al., 1996; Scandurra et al., 2021). As an explanation for this phenomenon, the cuprite was dissolved under the action of sulfuric acid, resulting in that sulfate residue was present on the mineral surface. The O1s curve-fitting spectra of cuprite after ozonation are shown in Fig. 10c, revealing that the binding energy of O (II) oxide species was decreased from 530.92 eV to 530.76 eV, and the reason for this chemical shift was that Cu^+ was oxidized to Cu^{2+} on the cuprite surface. As the binding energy of oxygen in CuO was lower than that in Cu_2O, the oxidation on the cuprite surface reduced the binding energy.

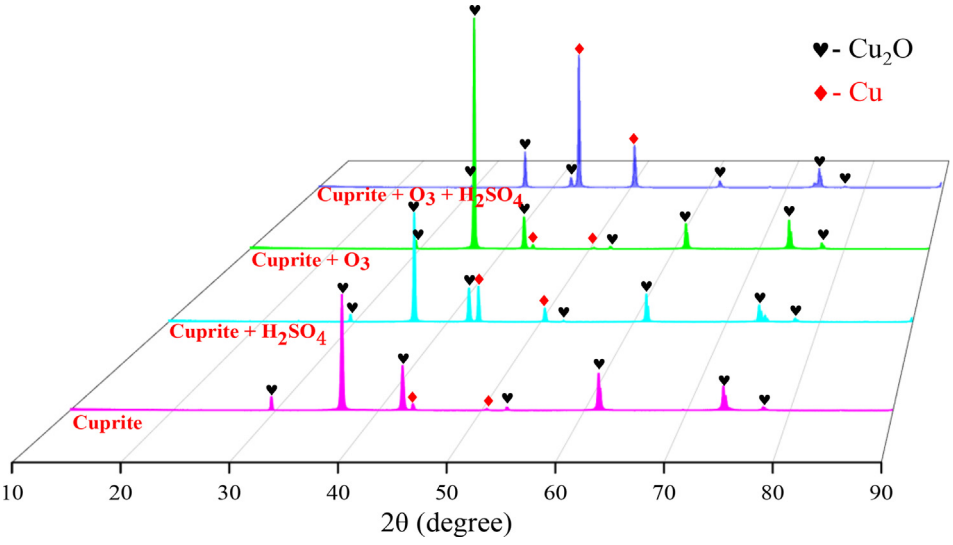

Fig. 9 X-ray diffraction patterns of raw cuprite, cuprite after direct leaching, cuprite after ozonation, and cuprite after oxidation leaching.

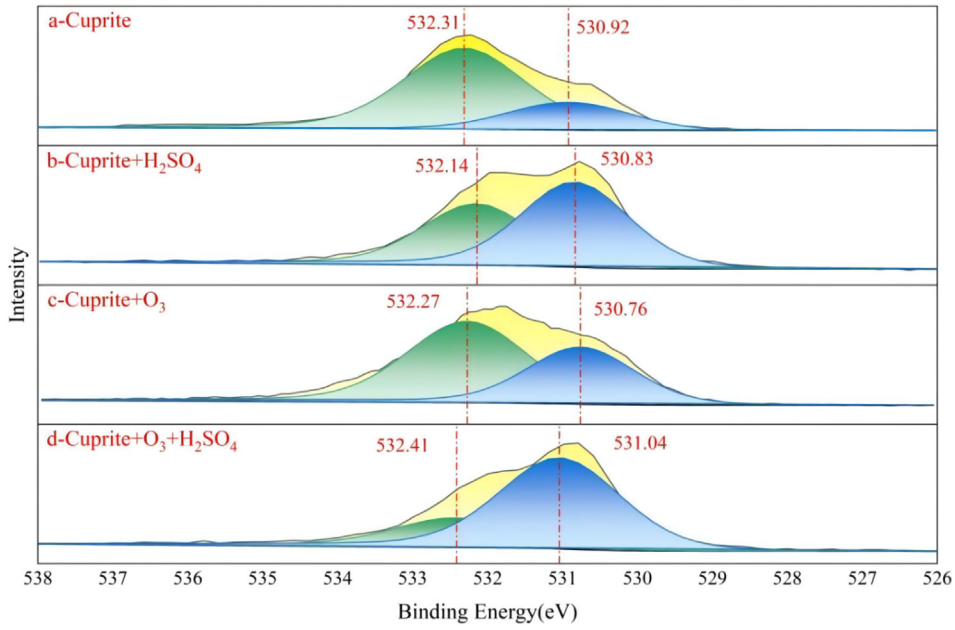

Fig. 10 XPS curve-fitting spectra of O 1 s: (a) cuprite, (b) cuprite + H_2SO_4, (c) cuprite + O_3, and (d) cuprite + O_3 + H_2SO_4.

Fig. 10d shows the O1s curve-fitting spectra on the cuprite surface after oxidation leaching for 20 min. It was clear that the change in the binding energy of metal oxides was extremely small, and the fresh surface after leaching was similar to that of cuprite. From the perspective of thermodynamics, sulfuric acid could easily dissolve CuO. Therefore, it was concluded that once each layer of Cu_2O on cuprite was oxidized to CuO, this CuO film could be dissolved in sulfuric acid.

Figure 11(a-d) shows the XPS spectra peaks of Cu 2p on the surface of cuprite without any treatment, after sulfuric acid leaching, after ozonation, and after oxidation leaching for 20 min, respectively. As shown in Fig. 11a, a peak at 932.79 eV was assigned to Cu_2O (Poulston et al., 1996; Scandurra et al., 2021). As shown in Fig. 11b, when the cuprite was leached by sulfuric acid, a dissolution reaction occurred, resulting in the chemical displacement; and further, Cu^0 and Cu^+ might be present on the cuprite surface. The XPS results of the cuprite after ozonation showed that the binding energy of Cu 2p3/2 could be fitted to two peaks, and peaks of 934.38 eV and 932.7 eV were assigned to CuO and Cu_2O, respectively (Fig. 11c) (Poulston et al., 1996; Scandurra et al., 2021). Therefore, it was easy to understand that ozone

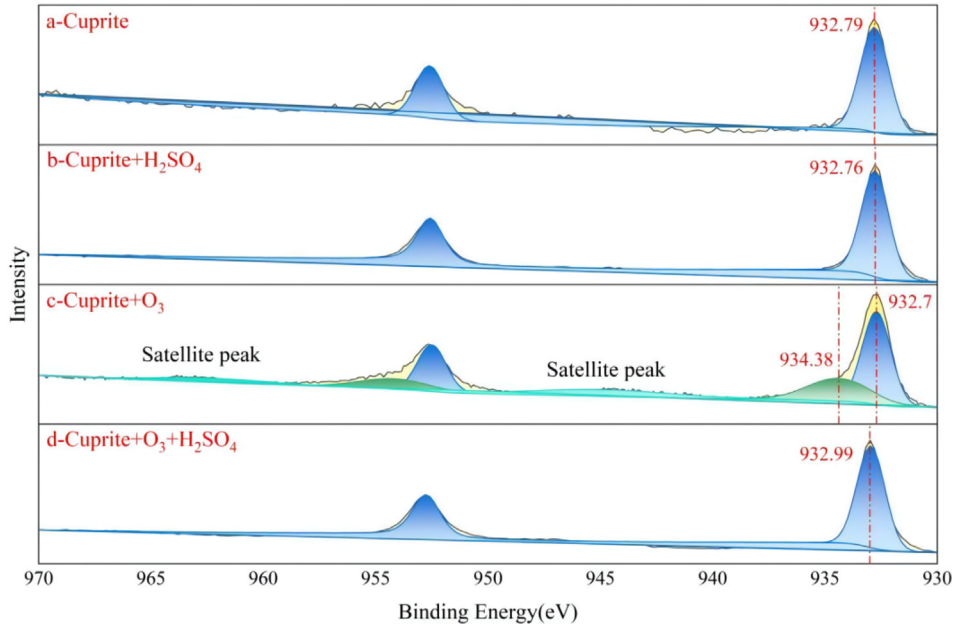

Fig. 11 XPS curve-fitting spectra of Cu 2p: (a) cuprite + DI water, (b) cuprite + H_2SO_4, (c) cuprite + O_3, and (d) cuprite + O_3 + H_2SO_4.

oxidized the cuprite, and part of Cu^{+} on the cuprite surface might be converted into Cu^{2+}. As shown in Fig. 11d, after both ozonation and sulfuric acid leaching, the surface spectrum peak of Cu 2p3/2 at 932.99 eV was basically similar to the peak of raw cuprite at 932.79 eV, indicating that the material on the mineral surface was still Cu_2O after oxidation leaching. Therefore, every time cuprite was oxidized to a layer of CuO film, sulfuric acid preferentially dissolved this layer of film, and this was definitely the cycle of oxidation leaching until cuprite was completely leached.

3.5. SEM-EDS analysis for morphology and chemical composition of raw cuprite, oxidative product and leaching residue

To further investigate the effect of direct leaching, ozonation, and oxidation leaching on the change of cuprite surface, the EDS area scanning analysis was performed on the surface, and the results are shown in Fig. 12. Fig. 12(b, d, f and h) shows the EDS spectrum of cuprite, cuprite after direct leaching using sulfuric acid, cuprite after ozonation, and cuprite after oxidation leaching, respectively.

As shown in Fig. 12a, the surface of raw cuprite was relatively smooth. The semi-quantitative analysis result from Fig. 12b shows that the weight concentrations of Cu atoms and O atoms were 89.97% and 10.03%, respectively, and they were basically consistent with the theoretical copper content in cuprite (88.82%). Fig. 12c shows that the surface topography of the cuprite changed significantly after direct leaching, and its surface became rougher. When the cuprite was directly leached by sulfuric acid, the weight concentration of Cu atoms increased from 89.97% to 94.58%, and correspondingly the weight concentration of O atoms decreased from 10.03% to 5.42%. This was due to the fact that the disproportionation reaction between cuprite and H^{+} occured to generate Cu, Cu^{2+}, and H_2O, which reduced the concentration of O atoms in cuprite after the leaching reaction, leading to the increased weight concentration of Cu atoms and the decreased weight concentration of O atoms.

During ozone oxidation, a large number of chiff-like substances appeared on the cuprite surface as shown in Fig. 12e. This might be resulted from the uneven oxidation on the cuprite surface, leading to the generation of an unevenly distributed oxide layer. The result of the semi-quantitative analysis for the cuprite after ozonation was similar to that for raw cuprite. Fig. 12g shows that the cuprite surface after oxidation leaching was uneven and rough, indicating that an intense oxidation leaching reaction. The semi-quantitative analysis for the oxidation leached cuprite showed that the weight concentration of Cu atoms was 96.51% and that of O atoms was 3.23%. In addition, 0.26% of S was found, due to the existence

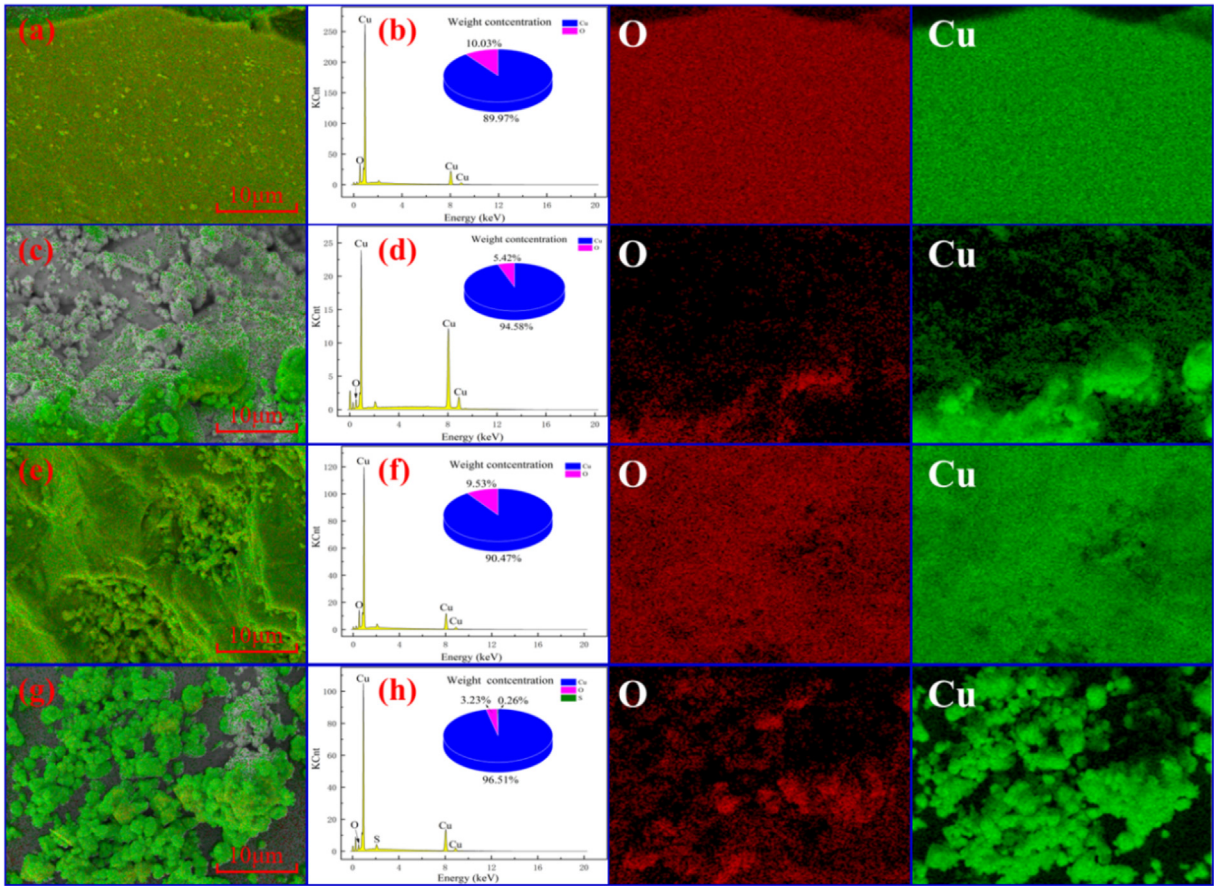

Fig. 12 SEM image and EDS spectra of cuprite samples: (a and b) untreated, (c and d) direct leaching, (e and f) ozonation, and (g and h) oxidation leaching.

of copper sulfate on the mineral surface. The copper content in the leaching residue after oxidation leaching was higher than that in other groups of EDS experiments, and two reasons might account for this result. First, raw cuprite contained a small amount of copper element, which was not leachable. Second, for an ideal oxidation leaching process, cuprite was oxidized first and then it was leached, but a small part of cuprite was directly leached by sulfuric acid before being oxidized in practice. However, as a disproportionation reaction for the direct leaching of cuprite, copper elements generate on the cuprite surface. Consequently, after the oxidation leaching of cuprite, only copper elements remained in the leaching residue, resulting in a high copper content (96.51%). It is clear that, these results were consistent with the XRD results.

3.6. ToF-SIMS analysis for surface chemical composition of raw cuprite, oxidative product and leaching residue

To further determine the effect of different agents on the cuprite surface, ToF-SIMS was particularly used to analyze

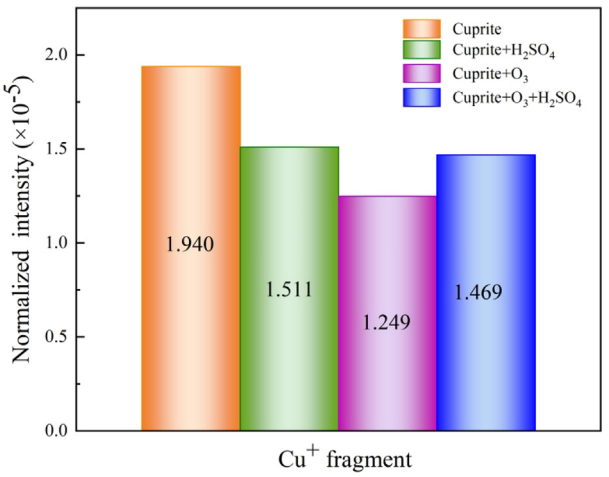

Fig. 14 Normalized intensity of Cu^+ secondary ions on surfaces of: (a) cuprite, (b) cuprite + H_2SO_4, (c) cuprite + O_3, and (d) cuprite + O_3 + H_2SO_4.

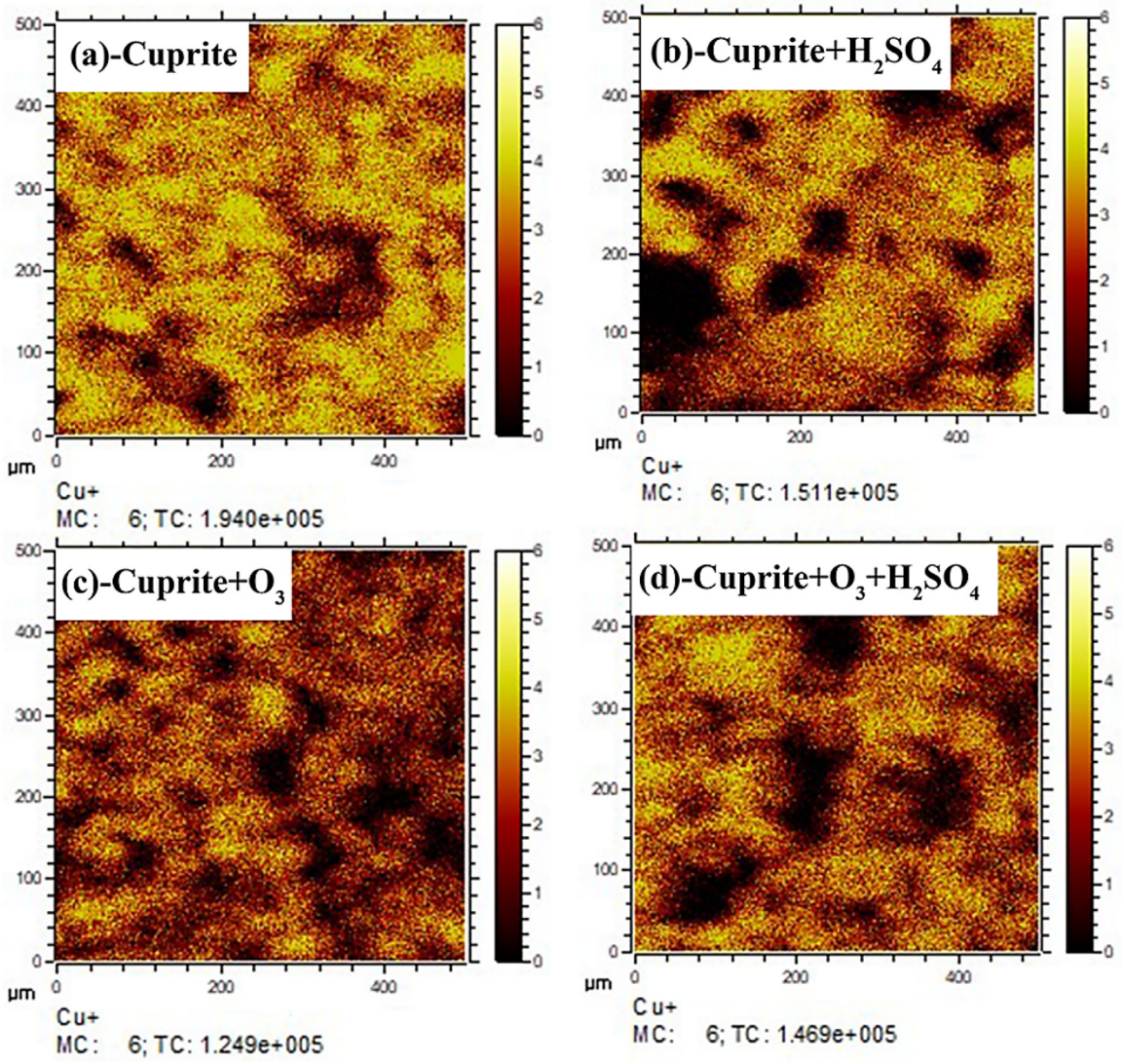

Fig. 13 Copper ion mass spectra in ToF-SIMS for samples: (a) cuprite, (b) cuprite + H_2SO_4, (c) cuprite + O_3, and (d) cuprite + O_3 + H_2SO_4.

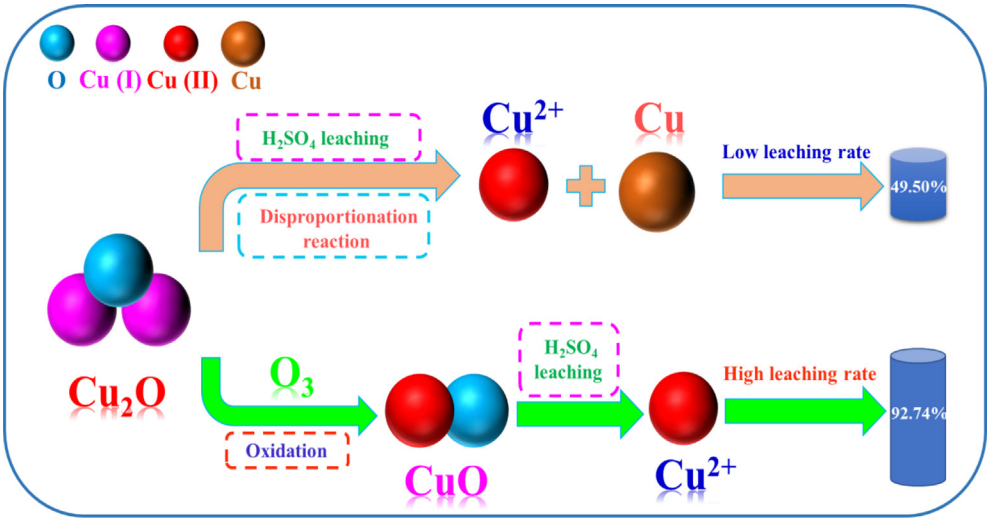

Fig. 15 A proposed oxidation leaching mechanism for cuprite by ozonation in sulfuric acid solution.

its surface chemical composition, by comparing their chemical compositions and normalized intensities (Lai et al., 2020).

The image of Cu^+ secondary ion fragments under different processing conditions for cuprite is shown in Fig. 13, and the normalized intensity of Cu^+ secondary ions on the cuprite surface under different conditions is shown in Fig. 14. As shown in Fig. 14a, the intensity of Cu^+ secondary ion fragments (1.940×10^{-5}) on the cuprite surface was the largest among the four groups. Fig. 14b illustrates that the intensity of Cu^+ secondary ion fragments on the cuprite surface was weakened to 1.511×10^{-5} after the direct leaching of cuprite with sulfuric acid. Obviously, this was because sulfuric acid dissolved a small amount of copper (I) in the cuprite. However, when cuprite was oxidized by ozone, the intensity of Cu^+ secondary ion fragments on the cuprite surface further decreased to 1.249×10^{-5}, as shown in Fig. 14c. In the ozonation process, ozone oxidized Cu^+ on the cuprite surface to Cu^{2+}, changing the ratio of Cu:O on the cuprite surface from the original 2:1 to 1:1. Therefore, compared with the raw cuprite, the oxygen content on the cuprite surface after ozonation increased, and the intensity of Cu^+ secondary ion fragments decreased. Compared with the direct leaching, the intensity of Cu^+ secondary ion fragments on the cuprite surface after oxidation leaching decreased from 1.511×10^{-5} to 1.469×10^{-5}, as clearly shown in Fig. 14d. The aforementioned results have fully confirmed that ozone effectively oxidized cuprite, changing Cu^+ to Cu^{2+} on the cuprite surface, and strengthened the leaching process for cuprite.

Based on the aforementioned results and analyses, a schematic diagram for the oxidation leaching of cuprite was proposed, as specifically shown in Fig. 15.

4. Conclusions

The oxidation leaching for cuprite using O_3 in sulfuric acid solution and its leaching mechanism were investigated. The results of leaching experiments demonstrated that Cu leaching rate was dramatically improved after the pretreatment with ozone for the cuprite, and the leaching process of cuprite controlled by mixed steps and the reaction activation energy was 31.51 kJ/mol.

The surface morphology of the cuprite after oxidation leaching has changed the most, and the oxidation leaching reaction was intense after pretreatment with ozone. The disproportionation reaction occurred in the direct leaching process for cuprite was mostly inhibited during its oxidation leaching process. Furthermore, ozone effectively oxidized Cu^+ on the cuprite surface to Cu^{2+}, and the oxidized cuprite exhibited enhanced solubility in the sulfuric acid solution because of the timely dissolution by sulfuric acid for the newly generated CuO film. The outcome from this investigation might provide a green approach for the effective oxidation leaching of cuprite.

CRediT authorship contribution statement

Jing Yang: Methodology, Data curation, Investigation, Writing – original draft. **Luzheng Chen:** Validation, Writing – review & editing, Supervision, Funding acquisition. **Dandan Wu:** Project administration, Conceptualization, Funding acquisition, Writing – review & editing. **Jing Cao:** Data curation, Validation. **Jinfu Guo:** Data curation.

Declaration of Competing Interest

The authors declare that they have no known competing financial interests or personal relationships that could have appeared to influence the work reported in this paper.

Acknowledgements

This research project was supported by the Ten Thousand Talent Plans for Young Top-notch Talents of Yunnan Province (No. YNWR-QNBJ-2019-131), the Yangtze River Scholar Program in Kunming University of Science and Technology (No. 109720190145), the High-Level Talent Recruitment Program of Yunnan Province (No. CCC21321005A) and Analysis and Testing Fund of Kunming University of Technology (No. 2020 M20192201105).

References

Abazari, R., Esrafili, L., Morsali, A., Wu, Y.H., Gao, J.K., 2021. PMo12@UiO-67 nanocomposite as a novel non-leaching catalyst

with enhanced performance durability for sulfur removal from liquid fuels with exceptionally diluted oxidant. Appl. Catal. B Environ. 283, 119582.
Ajiboye, E.A., Panda, P.K., Adebayo, A.O., Ajayi, O.O., Tripathy, B. C., Ghosh, M.K., Basu, S., 2019. Leaching kinetics of Cu, Ni and Zn from waste silica rich integrated circuits using mild nitric acid. Hydrometallurgy 188, 161–168.
Alrousan, D.M.A., Dunlop, P.S.M., 2020. Evaluation of ozone-based oxidation and solar advanced oxidation treatment of greywater. J. Environ. Chem. Eng. 8, 104309.
Aracena, A., Perez, F., Carvajal, D., 2018. Leaching of cuprite through NH4OH in basic systems. T. Nonferr. Metal. Soc. 28, 2545–2552.
Baek, J.H., Jeong, M.J., Hu, W.G., Chang, H.S., 2019. Passivation improvement of nitric acid oxide by ozone post-treatment for tunnel oxide passivated contacts silicon solar cells. Appl. Surf. Sci. 489, 330–335.
Bai, S.J., Fu, X.Y., Li, C.L., Wen, S.M., 2018. Process improvement and kinetic study on copper leaching from low-grade cuprite ores. Physicochem. Probl. Mi. 54, 300–310.
Bottone, A., Boily, J.F., Shchukarev, A., Andersson, P., Klaminder, J., 2022. Sodium hypochlorite as an oxidizing agent for removal of soil organic matter before microplastics analyses. J. Environ. Qual. 51, 112–122.
Chen, Y.H., Liu, R.J., Wu, X.N., Liu, Y., Fu, J.W., Ou, H.S., 2022. Surface characteristic and sinking behavior modifications of microplastics during potassium permanganate pre-oxidation. J. Hazard. Mater. 422, 126855.
Chen, Z.Y., Ye, G.H., Xiang, P.Z., Tao, Y.Y., Tang, Y., Hu, Y.J., 2022. Effect of activator on kinetics of direct acid leaching of vanadium from clay vanadium ore. Sep. Purif. Technol. 281, 119937.
Cui, Y., Li, Y.C., Wang, W.S., Wang, X.J., Lin, J., Mai, X.M., Song, G., Naik, N., Guo, Z.H., 2021. Flotation separation of acrylonitrile-butadienestyrene (ABS) and high impact polystyrene (HIPS) from waste electrical and electronic equipment (WEEE) by potassium permanganate surface modification. Sep. Purif. Technol. 269, 118767.
Funke, J., Prasse, C., Dietrich, C., Ternes, T.A., 2021. Ozonation products of zidovudine and thymidine in oxidative water treatment. Water. Res. X 11, 100090.
Ge, J.H., Liu, Z.F., Guan, M.H., Kuang, J.E., Xiao, Y.H., Yang, Y., Tsang, C.H., Lu, X.Y., Yang, C.Z., 2022. Investigation of the electrocatalytic mechanisms of urea oxidation reaction on the surface of transition metal oxides. J. Colloid. Interf. Sci. 620, 442–453.
Gomes, T., Angioletto, E., Quadri, M.B., Cargnin, M., Souza, H.M. D., 2022. Acceleration of acid mine drainage generation with ozone and hydrogen peroxide: Kinetic leach column test and oxidant propagation modeling. Miner. Eng. 175, 107282.
Gui, Q.H., Hu, Y.T., Wang, S.X., Zhang, L.B., 2022. Mechanism of synergistic pretreatment with ultrasound and ozone to improve gold and silver leaching percentage. Appl. Surf. Sci. 576, 151726.
Han, G., Wen, S.M., Wang, H., Feng, Q.C., 2021a. Surface sulfidization mechanism of cuprite and its response to xanthate adsorption and flotation performance. Miner. Eng. 169, 106982.
Han, G., Wen, S.M., Wang, H., Feng, Q.C., 2021b. Identification of copper-sulfide species on the cuprite surface and its role in sulfidization flotation. Colloid Surf. A 624, 126854.
Han, G., Wen, S.M., Wang, H., Feng, Q.C., 2021c. Sulfidization regulation of cuprite by pre-oxidation using sodium hypochlorite as an oxidant. Int. J. Min. Sci. Technol. 31, 1117–1128.
Han, G., Wen, S.M., Wang, H., Feng, Q.C., 2021d. Effect of ferric ion on cuprite surface properties and sulfidization flotation. Sep. Purif. Technol. 278, 119573.
Han, G., Wen, S.M., Wang, H., Feng, Q.C., 2021e. Enhanced sulfidization flotation of cuprite by surface modification with hydrogen peroxide. T. Nonferr. Metal. Soc. 31, 3564–3578.
He, J.F., Zhang, M.M., Chen, H., Guo, S.L., Zhu, L.T., Xu, J., Zhou, K., 2022. Enhancement of leaching copper by organic agents from waste printed circuit boards in a sulfuric acid solution. Chemosphere 307, 135924.
Lai, H., Deng, J.S., Liu, Z.L., Wen, S.M., Huang, L.Y., 2020. Determination of Fe and Zn contents and distributions in natural sphalerite/marmatite by various analysis methods. T. Nonferr. Metal. Soc. 30, 1364–1374.
Li, L.X., Zhang, C., Yuan, Z.T., Xu, X.Y., Song, Z.G., 2019. AFM and DFT study of depression of hematite in oleate-starch-hematite flotation system. Appl. Surf. Sci. 480, 749–758.
Lv, X., Zhao, H.B., Zhang, Y.S., Yan, Z.F., Zhao, Y., Zheng, H., Liu, W.Q., Xie, J.P., Qiu, G.Z., 2021. Active destruction of pyrite passivation by ozone oxidation of a biotic leaching system. Chemosphere 277, 130335.
Manoli, K., Li, R.B., Kim, J., Feng, M.B., Huang, C.H., Sharma, V. K., 2022. Ferrate(VI)-peracetic acid oxidation process: Rapid degradation of pharmaceuticals in water. Chem. Eng. J. 429, 132384.
Marchon, B., Carrazza, J., Heinemann, H., Somorjai, G.A., 1988. TPD and XPS studies of O2, CO2, and H2O adsorption on clean polycrystalline graphite. Carbon 26, 507–514.
Martinez, C.M., Flores, I.G.P., Hellin, P., Contreras, F., Fenoll, J., 2022. Ozonation for remediation of pesticide-contaminated soils at field scale. Chem. Eng. J. 446, 137182.
Poulston, S., Parlett, P.M., Stone, P., Bowker, M., 1996. Surface oxidation and reduction of CuO and Cu2O studied using XPS and XAES. Surf. Interface Anal. 24, 811–820.
Scandurra, A., Censabella, M., Boscarino, S., Grimaldi, M.G., Ruffino, F., Condorelli, G.G., Malandrino, G., 2021. Solid-state fabrication of Cu2O/CuO hydroxide nanoelectrode array onto graphene paper by thermal dewetting for high-sensitive detection of glucose. Phys. Status Solidi A 218, 2100389.
Sheng, Q.Y., Yin, W.Z., Li, D., Fu, Y.F., Xue, J.W., Yao, J., 2018. Improving the sulfidation-flotation of fine cuprite by hydrophobic flocculation pretreatment. Int. J. Min. Met. Mater. 25, 1256–1262.
Sheng, Q.Y., Yin, W.Z., Yang, B., Chen, K.Q., Sun, H.R., 2021. Promotion of oxidation pretreatment on sulfidation of cuprite surface and its contribution to flotation. Miner. Eng. 174, 107256.
Su, L.X., Gong, D., Jin, Y.M., Wu, D.A., Luo, W., 2022. Recent advances in alkaline hydrogen oxidation reaction. J. Energy Chem. 66, 107–122.
Sun, W.X., Guo, S.Q., Liu, Y., Sun, Z.X., Wei, W.J., Wei, X.X., Gao, L.B., Gao, Y.Z., 2022. The desulfurization of coal tar pitch with potassium permanganate oxidation method. Fuel 323, 124230.
Tan, J.H., Cheng, Z.Y., Zhang, J.X., Xiang, X., 2020. Surface modification and flotation improvement of ilmenite by using sodium hypochlorite as oxidant and activator. J. Mater. Res. Technol. 9, 3368–3377.
Tan, J.H., Cheng, Z.Y., Zhang, J.X., Xiang, X., 2022. Nucleation-Oxidation coupled technology for High-Nickel ternary cathode recycling of spent Lithium-ion batteries. Sep. Purif. Technol. 298, 121569.
Wei, N., Xu, D.H., Hao, B.T., Guo, S.W., Guo, Y., Wang, S.Z., 2021. Chemical reactions of organic compounds in supercritical water gasification and oxidation. Water Res. 190, 116634.
Wu, Y.H., Li, Y.W., Zhao, T., Wang, X., Isaeva, V.I., Kustov, L.M., Yao, J.M., Gao, J.k., 2022. Bimetal-organic framework-derived nanotube@cellulose aerogels for peroxymonosulfate (PMS) activation. Carbohyd. Polym. 296, 119969.
Xie, R.Q., Zhu, Y.M., Liu, J., Li, Y.J., 2021. The flotation behavior and adsorption mechanism of a new cationic collector on the separation of spodumene from feldspar and quartz. Sep. Purif. Technol. 264, 118445.
Xin, C.F., Xia, H.Y., Zhang, Q., Zhang, L.B., Zhang, W., 2021. Leaching of zinc and germanium from zinc oxide dust in sulfuric acid-ozone media. Arab. J. Chem. 14, 103450.

Xing, Y.W., Xu, M.D., Gui, X.H., Cao, Y.J., Babel, B., Rudolph, M., Weber, S., Kappl, M., Butt, H.J., 2018. The application of atomic force microscopy in mineral flotation. Adv. Colloid Interfac. 256, 373–392.

Zhang, H.Q., Chen, G.H., Cai, X., Fu, J.T., Liu, M.X., Zhang, P.F., Yu, H., 2021. The leaching behavior of copper and iron recovery from reduction roasting pyrite cinder. J. Hazard. Mater. 420, 126561.

Zhang, R., Hou, W., Wang, H.Q., Hu, E.M., Lei, Z.W., Hu, F., Zhou, W., Wang, Q.L., 2022. Oxidative leaching of sandstone uranium ore assisted by ozone micro-nano bubbles. J. Radioanal. Nucl. Ch. 331, 1645–1658.

Zhu, G.L., Zhao, Y.H., Zheng, X.Y., Wang, Y.H., Zheng, H.T., Lu, D.F., 2019. Surface features and flotation behaviors of spodumene as influenced by acid and alkali treatments. Appl. Surf. Sci. 507, 145058.